Inhibitors of SCF-Skp2/Cks1 E3 Ligase Block Estrogen-Induced Growth Stimulation and Degradation of Nuclear p27^{kip1}: Therapeutic Potential for Endometrial Cancer

Savvas C. Pavlides, Kuang-Tzu Huang, Dylan A. Reid, Lily Wu, Stephanie V. Blank, Khushbakhat Mittal, Lankai Guo, Eli Rothenberg,* Bo Rueda,* Timothy Cardozo,* and Leslie I. Gold

Departments of Pathology (K.M., L.I.G.), Medicine (S.C.P., K.-T.H., S.V.B., L.I.G.), and Biochemistry and Molecular Pharmacology (D.A.R., L.W., E.R., T.C.), Divisions of Translational Medicine (S.C.P., K.-T.H., L.I.G.) and Gynecological Oncology (S.V.B.), and New York University Cancer Institute (L.I.G.), New York University School of Medicine, New York, New York 10016; Vincent Center for Reproductive Biology (L.G., B.R.), Massachusetts General Hospital, Boston, Massachusetts 02114; and Department of Obstetrics, Gynecology, and Reproductive Biology (B.R.), Harvard Medical School, Boston, Massachusetts 02115

In many human cancers, the tumor suppressor, p27^{kip1} (p27), a cyclin-dependent kinase inhibitor critical to cell cycle arrest, undergoes perpetual ubiquitin-mediated proteasomal degradation by the E3 ligase complex SCF-Skp2/Cks1 and/or cytoplasmic mislocalization. Lack of nuclear p27 causes aberrant cell cycle progression, and cytoplasmic p27 mediates cell migration/metastasis. We previously showed that mitogenic 17-β-estradiol (E2) induces degradation of p27 by the E3 ligase Skp1-Cullin1-F-Box- S phase kinase-associated protein2/cyclin dependent kinase regulatory subunit 1 in primary endometrial epithelial cells and endometrial carcinoma (ECA) cell lines, suggesting a pathogenic mechanism for type I ECA, an E2-induced cancer. The current studies show that treatment of endometrial carcinoma cells-1 (ECC-1) with small molecule inhibitors of Skp2/Cks1 E3 ligase activity (Skp2E3LIs) stabilizes p27 in the nucleus, decreases p27 in the cytoplasm, and prevents E2-induced proliferation and degradation of p27 in endometrial carcinoma cells-1 and primary ECA cells. Furthermore, Skp2E3LIs increase p27 half-life by 6 hours, inhibit cell proliferation (IC_{50}, 14.3μM), block retinoblastoma protein (pRB) phosphorylation, induce G_1 phase block, and are not cytotoxic. Similarly, using super resolution fluorescence localization microscopy and quantification, Skp2E3LIs increase p27 protein in the nucleus by 1.8-fold. In vivo, injection of Skp2E3LIs significantly increases nuclear p27 and reduces proliferation of endometrial epithelial cells by 42%–62% in ovariectomized E2-primed mice. Skp2E3LIs are specific inhibitors of proteolytic degradation that pharmacologically target the binding interaction between the E3 ligase, SCF-Skp2/Cks1, and p27 to stabilize nuclear p27 and prevent cell cycle progression. These targeted inhibitors have the potential to be an important therapeutic advance over general proteasome inhibitors for cancers characterized by SCF-Skp2/Cks1-mediated destruction of nuclear p27. **(*Endocrinology* 154: 4030–4045, 2013)**

ISSN Print 0013-7227 ISSN Online 1945-7170
Printed in U.S.A.

Received August 13, 2013. Accepted September 5, 2013.
First Published Online September 13, 2013

For News & Views see page 3970

* E.R., B.R., and T.C. contributed equally to this work.

Abbreviations: APC/Cdh1, anaphase promoting complex/Cdh1; Cdk, cyclin-dependent kinase; CHX, cycloheximide; E2, 17-β-estradiol; ECA, endometrial carcinoma; ECC-1, ECA cells-1; EEC, endometrial epithelial cell; ER, estrogen receptor; IHC, immunohistochemical analysis; MTS, [3-(4,5-dimethylthiazol-2-yl)-5-(3-carboxymethoxyphenyl)-2-(4-sulfophenyl)-2H-tetrazolium, inner salt; p27, p27^{kip1}; PARP1, Poly[ADP-ribose] polymerase 1; Pg, progesterone; PH3, phosphohistone 3; pRB, retinoblastoma protein; SCF-Skp2/Cks1, Skp1-Cullin1-F-Box- S phase kinase-associated protein2/cyclin dependent kinase regulatory subunit 1; siRNA, small interfering RNA; Skp2E3LIs, small molecule inhibitors of SCF-Skp2/Cks1 E3 ligase activity; SRFLM, super resolution fluorescence localization microscopy; TBST, Tris-buffered saline containing 0.1% Tween 20; veh, vehicle.

An early event in carcinogenesis is loss of growth regulation. The cyclin-dependent kinase (Cdk) inhibitor, $p27^{kip1}$ (p27), inhibits cell proliferation by arresting cells in late G_1 phase of the cell cycle by specifically blocking cyclin E/Cdk2 activity to prevent phosphorylation of retinoblastoma protein (pRB) (1, 2). The importance of p27 binding to Cdk2 for its tumor-suppressive function was shown by the development of tumors of multiple organs in p27 knock-in mouse studies, in which the Cdk2 regulatory domain of p27 was deleted (3). The tumor suppressor function of p27 can switch to being oncogenic either by its loss from the nucleus via ubiquitin-mediated degradation or by its mislocalization to the cytoplasm (1, 4, 5), where p27 represses RhoA signaling, thereby affecting cytoskeletal organization, cell migration, and tumor metastasis (1, 6, 7). Phosphorylation of p27 on specific amino acids by different kinases controls its fate (1), and accordingly, high kinase activity associated with malignant cellular behavior obviates the antiproliferative effect of p27 (8–10). Phosphorylation on Thr187 by cyclin E/Cdk2 or MAPK is required for p27 ubiquitylation in the nucleus by the E3 ligase complex Skp1-Cullin1-F-Box- S phase kinase-associated protein2/cyclin dependent kinase regulatory subunit 1 (SCF-Skp2/Cks1), which targets p27 for subsequent proteasomal degradation (11–13). Phosphorylation on Ser10 facilitates p27 binding to chromosome region maintenance 1 (CRM-1) for nuclear export (14), and phosphoinositide 3-kinase/protein kinase B-dependent phosphorylation of p27 on T157 and T198 prevents nuclear reentry (9, 15, 16). Whereas low levels or loss of nuclear p27 and/or cytoplasmic mislocalization can serve as prognostic indicators of poor outcome in numerous human malignancies (1, 16), cytoplasmic expression particularly carries a poor prognosis in certain cancers, including of breast, prostate, and kidney (1, 16–20).

Previously, we showed that loss of nuclear p27 occurs early in 17-β-estradiol (E2)-induced type I endometrial carcinogenesis (85% of endometrial carcinomas [ECAs]) (11). In vitro, we showed that E2 induces MAPK (Erk1/Erk2)-mediated phosphorylation of p27 on T187 causing Skp2/Cks1-dependent proteasomal degradation of p27 to enable E2-induced proliferation of both primary endometrial epithelial cells (EECs) and ECA cell lines (13). Furthermore, consistent with the opposing effects of E2 and progesterone (Pg) on endometrial cell proliferation, we showed that Pg markedly increases nuclear p27 and inhibits proliferation by decreasing Skp2/Cks1 via degradation of this complex by the E3 ligase, anaphase promoting complex/Cdh1 (APC/Cdh1). These studies provided a novel mechanism, by which hormones regulate cell proliferation by degrading key proteins via the ubiquitin proteasome system. In addition, we have shown that TGF-β prevents p27 degradation as well, by increasing APC/Cdh1-mediated degradation of Skp2/Cks1, and that p27 is required for TGF-β-mediated inhibition of proliferation in EECs (21). Together, these studies provide compelling evidence that Skp2/Cks1-dependent degradation of p27 is an important molecular target to harness growth regulation of EECs and is linked to the pathogenesis of E2-induced ECA.

General proteasome inhibitors, such as Bortezomib, as a class of cancer therapeutics, have been marginally successful for only a few cancers (eg, multiple myeloma) (22–24), likely because they indiscriminately block ubiquitin proteasome system-mediated degradation of proteins, including both tumor suppressors and oncogenes (25). Three enzymes collaborate to transfer (E1), conjugate (E2), and ligate (E3) ubiquitin to a protein for targeted degradation by the 26S proteasome (26). The E3 ligases provide the specificity for ubiquitylation of proteins that signal their destruction, and thus, inhibitors of E3 ligases are ostensibly specific for their target substrates, such as tumor suppressors. To this aim, we previously used a novel drug-binding pocket-based approach involving structure-based discovery/virtual library screening on the published crystal structure of Skp2/Cks1 (27) to identify diverse small molecule inhibitors of SCF-Skp2/Cks1 E3 ligase activity (Skp2E3LIs) (28, 29). Although the SCF-Cullin1, Skp1, Ring Box 1 complex can combine with a number of recognition module E3 ligases with numerous target substrates, including oncogenes, the drug-binding pocket at the substrate-binding interface of the F-box E3 ligase Skp2/Cks1 has specificity for only the Cdk inhibitors, p27 and p21 (29). The Skp2E3LIs were shown to directly interact with Skp2 by blocking Skp2-dependent ubiquitylation of p27 and its subsequent degradation, without affecting the level of Skp2 and other components of the SCF complex (30).

The current study queries whether any of these inhibitors could specifically prevent the degradation of nuclear p27 without causing accumulation of p27 in the cytoplasm. We show that 2 of 5 Skp2E3LIs, designated as C2 and C20, increase nuclear p27, while simultaneously decreasing cytoplasmic p27, and inhibit proliferation in an ECA cell line, endometrial carcinoma cells-1 (ECC-1), and primary ECA cells. Similarly, by super resolution fluorescence localization microscopy (SRFLM), p27 nuclear protein cluster density is increased in cells treated with C2. Moreover, the Skp2E3LIs block both E2-induced proliferation and degradation of p27 in vitro in ECC-1 cells and in vivo, in EECs in an in vivo mouse model collectively, suggesting their direct functional interaction with Skp2/Cks1 and strong therapeutic potential for E2-linked ECA. Because p27 degradation due to aberrantly high levels of

Skp2 is a common molecular defect in human cancers and is associated with poor survival in ECA (31) and other cancers as well as resistance to chemotherapy (32–35), inhibiting nuclear Skp2/Cks1 E3 ligase-mediated degradation of p27 could be an improved approach compared with nonspecific inhibition of the proteasome for cancer therapy.

Materials and Methods

Cell culture and treatments

The ECA cell lines (derived from well-differentiated endometrioid type I ECAs) ECC-1 and HEC-1B cells (American Type Culture Collection) were cultured as previously described (13). Primary ECA cells from fresh ECA tissues from type I endometrioid tumors derived from hysterectomies of women ages 35–55 years performed at New York University Langone Medical Center and Bellevue Hospital were procured, separated from stromal cells, and adapted to tissue culture as previously described (11). The protocol was approved by The Institutional Review Board of New York University (H-9243), informed consent was obtained, and the samples were evaluated by 2 surgical pathologists and graded according to the WHO/FIGO (I-III) classification (36). Primary ECA cells were cultured as previously described (13). ECC-1 cells and primary ECA cells were grown to 70%–80% confluence, synchronized in serum-free media for 24 hours, and treated with 10μM Skp2E3LIs dissolved in 0.1% dimethyl sulfoxide (vehicle [veh] for 18 h or as indicated in the figures). The Skp2E3LIs, C5 (no. 6719837), C2 (no. 6544607), C16 (no. 6744881), C1 (no. 6281766), and L6 (no. 7839058), from ChemBridge Corp, and C20 (no. A067/0031209), from Ryan Scientific, have been previously characterized (30). To determine whether Skp2E3LIs, C2 and C20, block E2-induced degradation of nuclear and cytoplasmic p27, ECC-1 cells were plated, cultured, synchronized, and treated with either 1nM 17-β estradiol (E2) (Sigma), E2 plus the estrogen receptor (ER) antagonist, 10nM ICI182,780 (Zeneca Ltd), 10μM C2, 10μM C2 plus E2, 10μM C20, or 10μM C20 plus E2 for 18 hours. The effect of Skp2E3LIs, C2 and C20, on blocking E2-induced proliferation in ECC-1 cells was determined using the proliferation assay described below. The general proteasome inhibitor, lactacystin (1μM; Calbiochem) was used where indicated. To determine p27 half-life, ECC-1 cells were cultured, synchronized, and treated with C2, C20, or veh for 18 hours, as described above, washed with media, and cycloheximide (CHX) (20μM) was added as a chase. Whole-cell lysates were collected at increasing time points (0, 2, 4, and 6 h), and 20-μg protein/well was analyzed for p27 by immunoblotting.

Super resolution fluorescence localization microscopy

Direct excitation fluorescence localization microscopy (37) was used to acquire pixel data that were then transformed into superhigh resolution images (38). ECC-1 cells, at a density of 1.2×10^5/slide, were seeded on gelatin-coated (2%) glass slides (gelatin type B; Sigma). The cells were grown to 60% confluency, synchronized by serum starvation for 24 hours and treated with the Skp2E3LI, C2 (10μM) for 18 hours, or veh (0.1% dimethyl sulfoxide). Cells were washed with PBS, treated with cold Extraction buffer (10mM HEPES-KOH [pH 7.4], 300mM sucrose, 100mM NaCl, 3mM $MgCl_2$, and 0.5% Triton X-100) for 2 minutes to remove the cytoplasm, washed with PBS, and fixed with 4% paraformaldehyde for 30 minutes. Nonspecific binding sites were blocked with 2% glycine, 2% BSA, 0.2% gelatin, and 50mM NH_4Cl in PBS for 60 minutes at room temperature, and the slides were incubated overnight at 4°C with mouse antihuman p27 (1:300, clone 57; BD Transduction Labs) or rabbit antihuman p45/Skp2 (1:300, clone H-435; Santa Cruz Biotechnology, Inc). Secondary antibodies coupled to Alexa Fluor 568 for Skp2 and Alexa Fluor 647 for p27 were incubated with the slides for 30 minutes. A custom-built microscopy setup (39–41), based on a Leica DMI3000 microscope equipped with an HCX PL APO 63X NA 1.47 OIL CORR total internal reflection fluorescence microscopy objective followed by achromatic ×2 tube lens magnification, was used; total magnification was ×126. The samples were excited at 532 and 645 nm by lasers in highly inclined illumination mode (42).

Dual-color acquisition and mapping error

The 2 channels (colors) were imaged simultaneously, side by side, onto a single EM-CCD camera (Andor iXon+897) acquiring at 33 Hz. Sample emission was collected and split into 2 channels by dichroic mirror and narrow-band emission bandpass filters (filter for green channel 580/60, filter for red channel 680/40; Semrock) by using a Dual View (DV2 Photometrics). For accurate alignment and mapping of the 2 color channels, diffraction-limited fluorescent beads were first imaged with emission spectra spanning both channels (Invitrogen). The location of the beads was matched for both channels, and a mapping matrix was generated using an IDL (Exelis Visual Information Solutions) custom mapping routine (39, 40, 43–45). This mapping matrix superimposes the 2 sides of the image, each corresponding to a different color, into a 2-color image, and the images obtained were processed and analyzed using an ImageJ macro routine, which is based on the QuickPALM plugin (46). For this analysis, each color is reconstructed at 20 nm/pixel using the following QuickPALM parameters: full width half maximum = 4 and signal/noise = 2.00, resulting in a superresolved image. These images from each color channel were than superimposed to generate a 2 color superresolved image; the mapping error in this image was 20 nm. The 2 color mapping error obtained was found to be better than 20 nm, as we and others previously reported (39, 40, 43–45).

Imaging and particle analysis

Imaging was performed using a buffer containing 100 mM mercaptoethylamine and an oxygen scavenging system (0.1-mg/mL glucose oxidase, 0.02-mg/mL catalase, and 0.8% [wt/wt] glucose), combined with appropriate laser excitation (37). Movies containing 2000 frames were used to generate reconstructed superresolved images. Particle analysis was performed using ImageJ software. Images were processed with a smoothing filter, adjusted for brightness and contrast, clipped into individual nuclei, and filtered to a threshold to obtain a binary image. Protein/cluster detection and parameters were obtained using the function "analyze particles" for the number of particles and their area. Density of particles was obtained by dividing the particle count by the excised area of the clipped nuclei.

Cell proliferation, viability, cell cycle, and apoptosis assays

ECC-1 cells and, separately, primary ECA cells were seeded in 96-well plates (BD Biosciences) at a density of 4×10^3/well and 3×10^4, respectively, grown to 70%–80% confluence, synchronized in serum-free media for 24 hours, and treated with increasing doses of C2, C5, and C20 (0.1μM–10μM), in triplicate, as described above, and cell proliferation was determined by the CellTiter 96 Aqueous One Solution (MTS, [3-(4,5-dimethylthiazol-2-yl)-5-(3-carboxymethoxyphenyl)-2-(4-sulfophenyl)-2H-tetrazolium, inner salt) assay (Promega). Values were calculated as percent of veh-treated control ± SD, as described (21). Propidium iodide staining followed by fluorescence-activated cell sorting was used for cell cycle distribution, as described (13). The half maximal effective concentration of C2 in inhibiting proliferation of ECC-1 was obtained by treating and analyzing the cells, as described above for determining growth inhibition, and analyzing the values derived as percent of veh-treated control with the hillslope method, which characterizes the slope of the curve at the midpoint, using GraphPad Prism software to determine the variable slope dose. The hillslope experiment is graphed on a logarithmic scale representing the increasing concentrations of C2 treatment. Cytotoxicity of the Skp2E3LIs was determined by plating the ECC-1 cells at a density of 1.5×10^5/well in 12-well plates (BD Biosciences), growing and synchronizing the cells as described above. The cells were treated with 10μM Skp2E3LIs (C5, C2, C20, C16, C1, and L6) for 48 hours, supernatants collected by centrifugation, adherent cells obtained by trypsinization, and the number of dead cells per 100 was determined by trypan blue (Invitrogen) exclusion and cell counting. The values (y axis) were determined as percent of veh control. The effect of Skp2E3LIs on apoptosis was determined by culturing, synchronizing, treating ECC-1 cells with 10μM Skp2E3LIs for 18 hours, and analyzing for caspase-3 cleavage and Poly[ADP-ribose] polymerase 1 (PARP1) cleavage by immunoblotting.

Immunoblot analysis

Whole-cell lysates were prepared in ice-cold radioimmunoprecipitation assay buffer (50mM Tris-HCL, 150mM NaCl, 0.25% sodium deoxycholate, 1% Nonidet P-40, and 1mM EDTA) containing 1mM Na_3VO_4 [pH 7.4]) and 1× protease inhibitor cocktail (Sigma Chem). After freezing and thawing, soluble proteins were obtained by centrifugation. Protein concentrations were quantified (BCA kit; Thermo Scientific), and 20-μg protein in Laemmli buffer was subjected to SDS-PAGE (12.5% polyacrylamide) and immunoblotted using anti-p27 and anti-Skp2 antibodies to probe protein levels, as described (13, 21). Subcellular fractionation was performed using the NE-PER kit (Thermo Scientific), and 10-μg cytoplasmic and nuclear protein fractions were used for immunoblotting. The nitrocellulose membranes were blocked with 5% nonfat dry milk in Tris-buffered saline (TBS) containing 0.1% Tween 20 (TBST) or in 3% BSA in TBST for phospho-pRb for 1 hour, incubated overnight with mouse antihuman p27 (1:1000, clone 57; BD Transduction Labs), mouse antihuman p45/Skp2 (1:1000, clone 8D9; Invitrogen), rabbit antihuman phospho-pRb (1:500; Santa Cruz Biotechnology, Inc), mouse antihuman pRb (1:500, clone 2; BD Transduction Labs), rabbit antihuman caspase-3 (1:500, clone 8G10; Cell Signaling Technology), or rabbit antihuman PARP1 (1:500; Cell Signaling Technology). Purity of the subcellular fractions was confirmed using mouse antihuman α-tubulin (1:10 000, clone B-5–1-2; Sigma) or rabbit antihuman specificity protein 1 (1:1000, clone H-225; Santa Cruz Biotechnology, Inc) for the cytoplasmic and nuclear fractions, respectively. Secondary antibodies were peroxidase-conjugated goat antirabbit or goat antimouse in TBST (1:2000; Thermo Scientific). The blots were reprobed with mouse anti-β-actin (1:10 000, clone AC15; Sigma) as loading control. Protein bands were resolved using the SuperSignal West Dura kit (Thermo Scientific), visualized by exposure to x-ray film (HyBlot; Denville Scientific), and after densitometric scanning (Kodak Logic-100), the protein bands were quantified by normalizing to β-actin and then compared with the untreated control. The values represented by the graphs of relative protein levels compared with β-actin in each well, shown as percent of veh control, are expressed as relative intensity of each band ± SD and are the averages of at least 3 separate experiments.

RNA interference

Skp2 was knocked down in ECC-1 cells with *Skp2* small interfering RNA (siRNA) or treated with control siRNA exactly as previously described (13). To determine the effect of Skp2E3LIs, C2 and C20, on p27 levels after knocking down of Skp2, 24 hours after transfection, the cells were synchronized and treated with C2 and C20, subjected to subcellular fractionation, and analyzed by immunoblotting. To determine the effect of C2 and C20 on cell proliferation after knock-down of Skp2, the cells were seeded in 96-well plates at a density of 1×10^4 in complete media, transfected, synchronized, treated with C2 and C20, and cell proliferation determined, as described above.

Treatment of mice with Skp2E3LIs and immunohistochemical analysis (IHC) for p27 and phosphohistone 3 (PH3)

Two-month-old female C57BL/6 mice were ovariectomized and 2 weeks later injected sc with E2 in sesame oil (100 ng/mouse) for 2 consecutive days followed by no treatment for 2 more days. Subsequently, one Skp2E3LI (10 μg/ml; C2, and C5) in veh (0.5% methylcellulose, 0.2% Tween) or veh alone was injected into the mice ip once for 2 consecutive days (d 5 and 6), and the mice euthanized 16 hours after the last injection (d 7). One uterine horn was excised, fixed in 4% paraformaldehyde, embedded in paraffin, and placed on slides for IHC for p27 and PH3 (n = 4 mice/treatment arm; n = 1 experiment). This study was approved by the Massachusetts General Hospital Subcommittee on Research and Animal Care.

Immunohistochemical analysis

IHC was performed, as previously described (11) and as per the Vectastain ABC Elite kit (PK6100; Vector Laboratories). Antigen retrieval (Biogenex) was used before incubating the slides with anti-p27 or anti-PH3 antibodies. The p27 primary antibody (1:100 in kit blocking buffer, catalog no. sc-528; Santa Cruz Biotechnology, Inc) or PH3 antibody (Ser10; 1:200, catalog no. 06–570; Millipore) was incubated with the slides overnight at 4°C. Rabbit polyclonal IgG (1:100) was used as a negative control (catalog no. AB27478; Abcam), and goat antirabbit IgG was the secondary antibody (1:200, catalog no. sc-2040; Santa Cruz Biotechnology, Inc). 3,3′-diaminobenzidine was used for detection (catalog no. K3468; Dako). Positive nuclei for p27 or

PH3 were counted in 3 separate fields and expressed as the number of nuclei per 100 cells.

Statistical analysis

All proliferation, toxicity, and IHCs for p27 and PH3 are presented as means ± SD. A 2-tailed, paired Student's *t* test was used to predict statistical significance of the comparison between 2 means. Results are significant at $P \leq .05$ at 95% confidence level using GraphPad Prism software.

Results and discussion

Skp2E3LIs increase nuclear p27

An array of the Skp2E3LIs was previously shown to have differential effects in cell based assays using cell lines from different cancers in terms of the degree of p27 stabilization and cell cycle effects (30). Because we previously have shown that p27 is an important molecular target for growth arrest in primary EECs and ECA cell lines (11, 13, 21, 47), we first determined whether Skp2E3LIs could increase p27 in an ECA cell line, ECC-1. As shown in Figure 1A, 4 out of 5 Skp2E3LIs added to cells at 10 μM for 18 hours increase the levels of p27 by 2–2.5-fold. Although it has been thought that Skp2 is localized in the nucleus where it ubiquitylates p27 (48, 49), we and others have shown that Skp2 can reside in the cytoplasm (13, 50, 51) and, also, that E2 increases and Pg decreases Skp2 in both subcellular compartments with an inverse effect on the levels of nuclear and cytoplasmic p27 (13). The optimal concentration of C2 and C20 that increases p27 was 10μM (2.3- and 2.2-fold over control, respectively) (Figure 1B), with no further increase at 20μM (Supplemental Figure 1, published on The Endocrine Society's Journals Online web site at http://endo.endojournals.org). C2 and C20 had little to no effect on the levels of Skp2, confirming their specificity for Skp2 E3 ligase activity (Figure 1B). Importantly, we assessed whether any of the Skp2E3LIs could specifically increase nuclear p27, because accumulation of cytoplasmic p27 would be an adverse effect of these potential therapeutic agents (1, 4–6). Figure 1C shows that treatment of ECC-1 cells with C2 and C20 for 18 hours specifically increases nuclear p27 by 1.8- and 2.2-fold, respectively, compared with veh control. Supplemental Figure 2 shows a similar 1.8-fold increase in nuclear p27 in response to C5. In contrast, C1 and C16 increase p27 in both the nucleus by 2.3- and 2.2-fold, respectively, and in the cytoplasm by 2.5- and 2.7-fold, respectively. This is identical to lactacystin, a general proteasome inhibitor (ie, Bortezomib), which increases p27 in both subcellular fractions (Figure 1D). Therefore, the Skp2E3LIs, C5, C2, and C20, specifically increase nuclear p27.

SRFLM imaging was used to determine the effect of the Skp2E3LI, C2, on the spatial organization and relationship between p27 and Skp2 in situ in the nuclei of ECC-1 cells. This technique subverts the resolution limits inherent in conventional light microscopy allowing for visualization of proteins with more than 10-fold higher, near molecular resolution (38, 52). Because precise molecular shapes and locations relative to cellular ultrastructure can be obtained by SRFLM, small differences in the in situ cellular configurations of these proteins in the nucleus can be observed in response to Skp2E3LI activity (as shown in Figure 2, A and C, right panels, compared with the raw fluorescence image, left panels). SRFLM (Figure 2, A and C, right panels) reveals a discrete nuclear organization of p27 (pink) and Skp2 (green) in veh (Figure 2A) and C2-treated cells (Figure 2C). Areas of unique (pink or green) and co (white-yellow)-localization of p27 and Skp2 are observed in both the veh-treated (Figure 2B) and C2-treated cells (Figure 2D). The density or distribution of p27 protein clusters in the nucleus (clusters per nm^2) is not changed by C2 treatment (Figure 2E). However, the average size of the clusters is significantly increased (1.8-fold increase) (Figure 2F). This means that C2 treatment of the cells induces an increase in the amount of p27 in the nucleus in the form of greater aggregation at specific sites already present in the nucleus rather than the appearance of more numerous protein clusters. Plotting the histogram of cluster sizes shows that larger p27 clusters are rare, and the increase in the average size derives from increases in the largest clusters but not all clusters (Figure 2G). Along with the data on the activity of C2 and its specificity for p27 degradation inhibition (30), this observation suggests that a threshold p27 cluster size is necessary for G_1 arrest and that just a few clusters reaching this threshold size in the nucleus is sufficient to arrest the cell cycle. The density of Skp2 clusters is also not changed by C2 treatment, and their average size is increased but not as significantly (Figure 2, H and I). The increase in p27 protein and slight increase in Skp2 in response to C2 observed by SRFLM is consistent with the amounts of these proteins obtained in Figure 1C by immunoblotting. Unlike p27, however, the histogram of Skp2 clusters is bimodal with a second peak of clusters around 30 000–50 000 nm^2 size (Figure 2J), but this distribution is relatively unaffected by C2 treatment. This distribution suggests the ubiquitous (rather than cell cycle phase specific) presence of 2 different forms of Skp2 clusters, the second being a higher-order oligomeric structure. Because Skp2 has several substrates, it is possible that only 1 of the 2 detected forms is specific for p27. Future SRFLM studies may confirm the molecular environment of these Skp2 forms within chromatin, eg, relative to the location of origins of DNA replication. These studies dem-

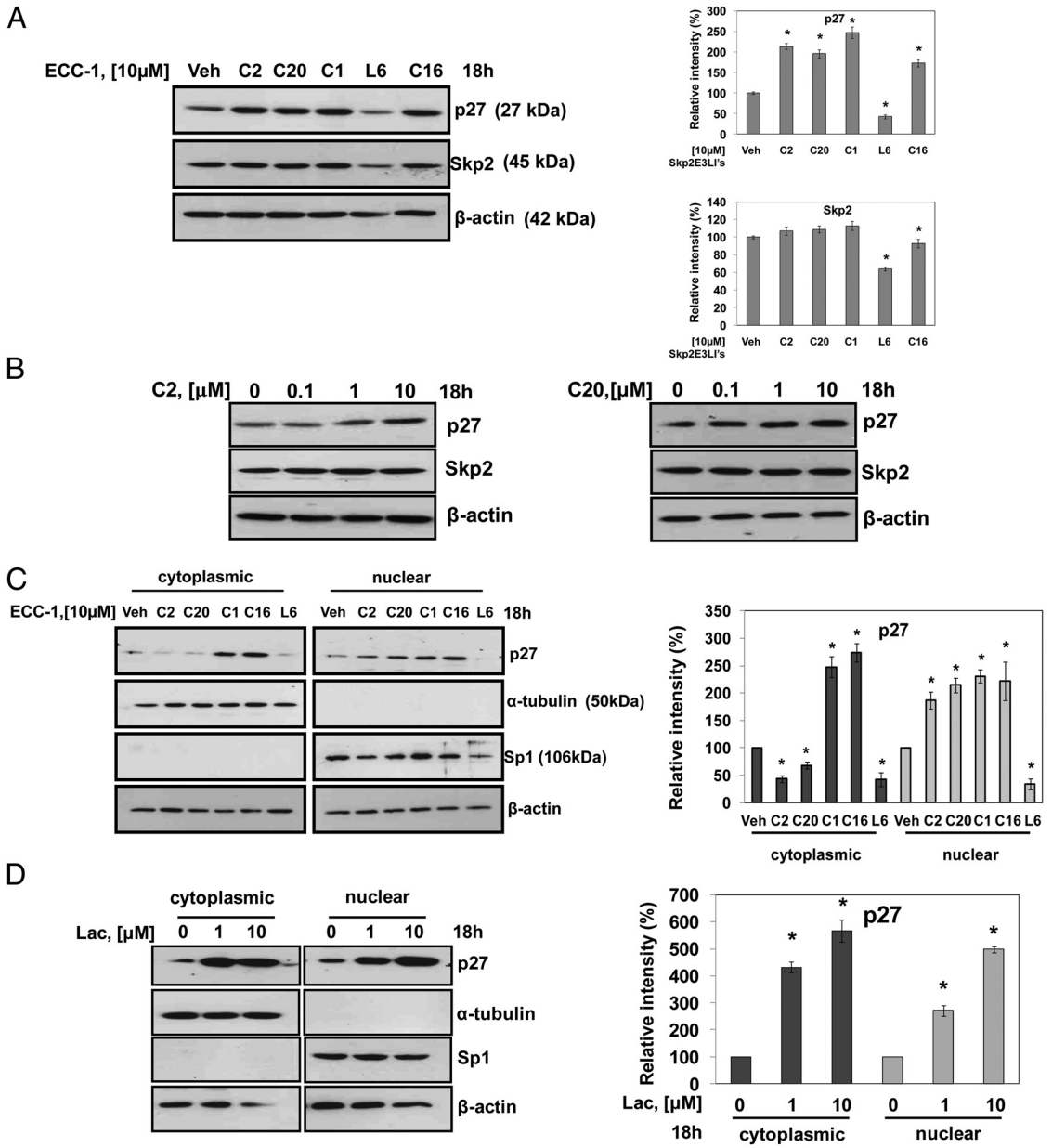

Figure 1. Skp2E3LIs increase nuclear p27 in the ECA cell line, ECC-1. (A) The Skp2E3LIs, C2, C20, C1, C16, but not L6, increase p27 protein levels in ECC-1 cells over veh control. Cells were treated with Skp2E3LIs and whole-cell lysates immunoblotted, n = 3 experiments. The graphs depict densitometry of relative intensity of bands for p27 and Skp2 normalized to the corresponding β-actin and compared with veh (100%). (B) Dose-dependent response to C2 and C20, with no effect on the levels of Skp2. Cells were treated and analyzed by immunoblotting (n = 4). (C) C2 and C20 specifically increase nuclear p27, whereas C1 and C16 increase cytoplasmic and nuclear p27, over veh. Antibodies to α-tubulin and specificity protein 1 confirm purity of cytoplasmic and nuclear fractions, respectively. The graph, reflecting densitometry of bands, shows relative intensity of p27 levels normalized to β-actin (veh, 100%; n = 2). (D) Lactacystin, increases both nuclear and cytoplasmic p27. The graph shows relative intensity of p27 levels normalized to actin (veh, 100%; n = 3). Densitometry of protein bands is shown as an average of all blots for the number of experiments performed; a representative blot is shown; statistical significance, *, $P \leq .05$. Details for all figures are in Materials and Methods.

onstrate the utility of SRFLM used in conjunction with specific target-based chemical probes, such as Skp2E3LIs.

Skp2E3LIs that increase nuclear p27 inhibit proliferation, block phosphorylation of pRb, and induce G_1 phase block

As shown in Figure 3A, C5, C2, and C20 are functionally active in ECC-1 cells at the concentration causing maximal accumulation of p27 (10μM), showing a statistically significant inhibition of proliferation of 29% ($P \leq .004$), 33% ($P \leq .012$), and 30% ($P \leq .019$), respectively, over the veh control; no greater effect on proliferation was observed with 20μM (data not shown). The extent of inhibition of proliferation is similar to previous studies using TGF-β and Pg with a similar 2-fold increase in nuclear p27 (13, 21). We compared TGF-β and Pg, at their previously

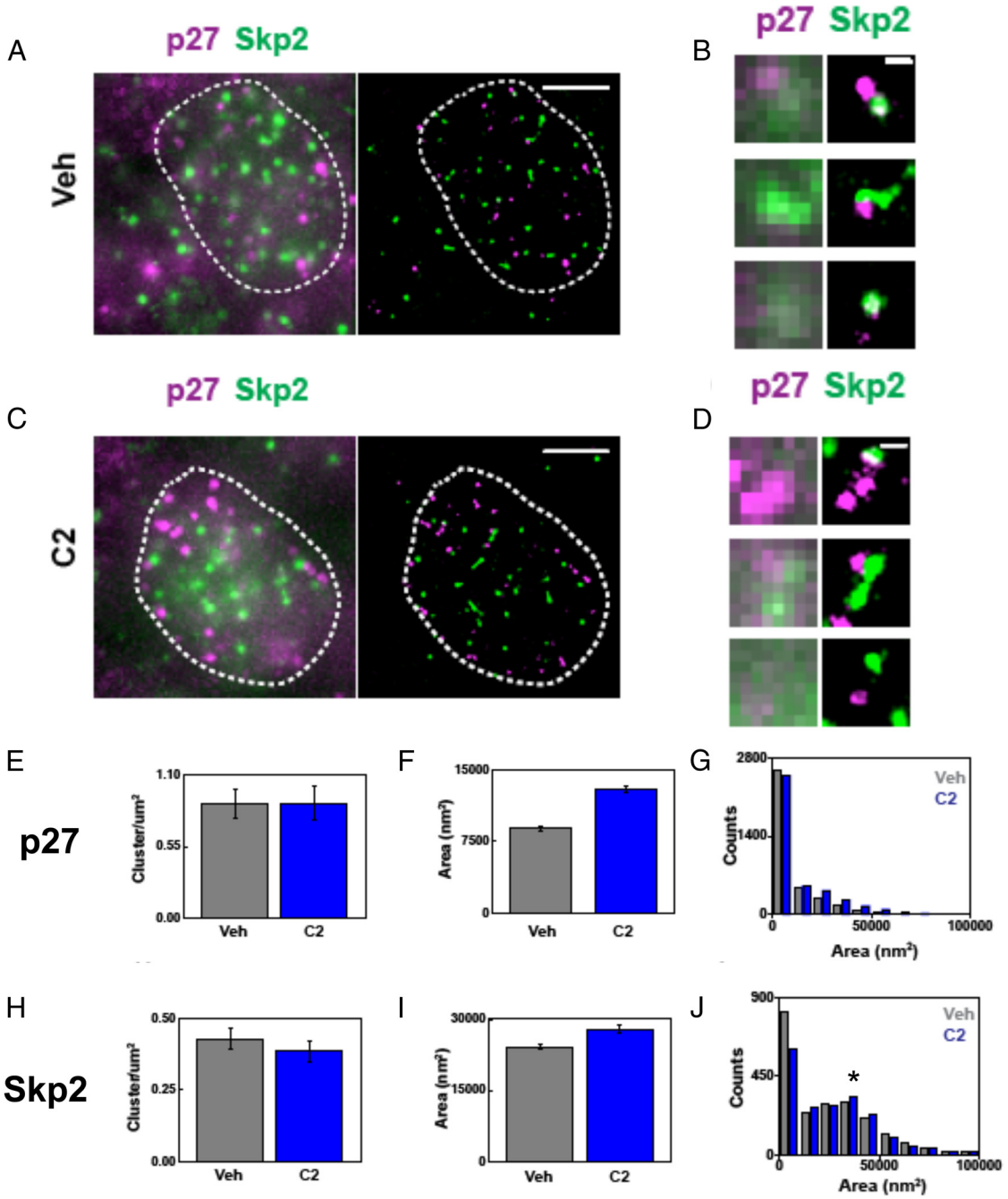

Figure 2. Skp2E3LI, C2, increases nuclear p27 in ECC-1 cells determined by super resolution fluorescent microscopy and quantitation. (A) ECC-1 cells were treated with C2, or veh for 18 hours and prepared as described in Materials and Methods. (A) One representative ECC-1cell nucleus treated with veh is outlined (white dashed line) in both a raw total internal reflection fluorescence (TIRF) image (left panel) and super resolved image (right panel). The scale bar corresponds to 3 μm. (B) Selected zoomed regions from the cell treated with veh (panel A) show colocalization between p27 and Skp2 in both TIRF and super resolution formats. The scale bar corresponds to 300 nm. (C) One representative ECC-1 cell nuclei treated with C2 is outlined (white dashed line) in both a raw TIRF image (left panel) and super resolved image (right panel). The scale bar corresponds to 3 μm. (D) Selected zoomed regions from the C2-treated cell in C show colocalization between p27 and Skp2 in both TIRF and super resolution formats. The scale bar corresponds to 300 nm. Both B and D resolve p27 and Skp2 in a complex. (E and H) The protein/cluster density of p27 (E) and Skp2 (H) in ECC-1 cell nuclei treated with veh (n = 39 nuclei counted) or C2 (n = 40 nuclei counted) is unchanged. Error bars correspond to the SEM. (F and I) C2 significantly increases the area of protein clusters for p27 (F) compared with veh-treated cells; there is a slight nonstatistically significant increase in Skp2 (I) compared with veh-treated cells. Error bars correspond to SEM. (G and J) C2 induces an increase in p27 cluster area distribution (size) by associating with existing nuclear p27 (G) clusters, whereas Skp2 (J) shows 2 populations; both are compared with veh-treated cells. The data in J shows that after C2-treatment, Skp2 forms a higher-order oligomeric structure with a peak in area at 40 000 nm^2.

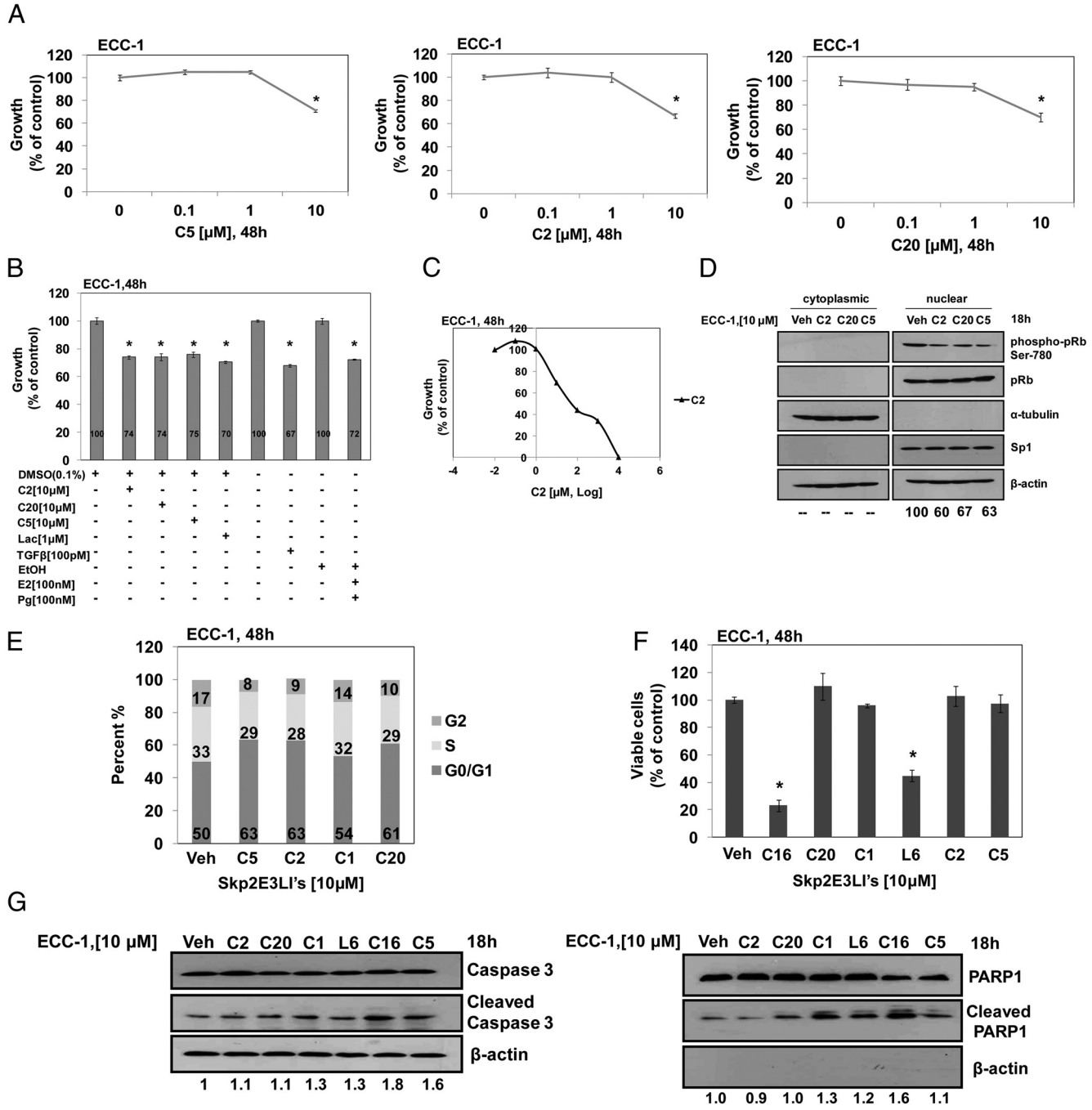

Figure 3. The Skp2E3LIs, C5, C2, and C20, inhibit cell proliferation, block cells in G_1, are not cytotoxic, and do not induce apoptosis in ECC-1 cells. (A) Skp2E3LIs, C5, C2, and C20, inhibit cell proliferation. MTS assay was used to analyze for proliferation of ECC-1 cells; values were calculated as percent of veh-treated control ± SD, as described (21), and statistical significance was determined using GraphPad Prism software; *$P \leq .05$ (n = 4). (B) Skp2E3LIs C5, C2, and C20 inhibit proliferation of ECC-1 cells to a similar extent as TGF-β and Pg by MTS assay (described above). Values were calculated as percent of veh-treated cells and statistical significance determined using GraphPad Prism software; *, $P \leq .05$ (n = 3). (C) The EC_{50} of C2 in inhibiting proliferation of ECC-1 is 14.3μM. Values obtained as percent of veh-treated control and EC_{50} calculated using the hillslope method (n = 2). (D) C2, C20, and C5 block phosphorylation of nuclear pRb. Synchronized ECC-1 cells were treated with Skp2E3LIs for 18 hours, the cells subjected to subfractionation, and lysates immunoblotted for phospho-pRb (Ser-780) and pRb (n = 2). (E) C5, C2, and C20 increase the percentage of cells in G_0/G_1. Cell cycle distribution is presented as percent of cells in phases of the cell cycle. (F) C2, C20, C5, and C1 are not cytotoxic for ECC-1 cells. Cell viability calculated as percent of untreated control. Significance, *, $P \leq .05$ (n = 2). (G) C2 and C20 do not induce apoptosis. Apoptosis was determined in whole-cell lysates by PARP1 and caspase-3 cleavage (n = 3). Densitometric values in fold change over the veh-treated control are shown below each lane on the blot.

shown peak concentrations for inhibition of proliferation, with the Skp2E3LIs in the same experiment and show a similar result by TGF-β (33%; $P \leq .0026$), Pg (28%; $P \leq .0026$), and the Skp2E3LIs, C2, C20, and C5, by 26% ($P \leq .0015$), 26% ($P \leq .0049$), and 25% ($P \leq .0039$), respectively (Figure 3B). Interestingly, although lactacystin treatment greatly increases nuclear p27 (nearly 5-fold over veh) (Figure 1D), inhibition of proliferation is also in a similar range at 30% ($P \leq .00107$). In addition, the combination of each Skp2E3LI with Pg or TGF-β did not result in greater inhibition of proliferation (data not shown). It is important to note that a higher magnitude of inhibition of proliferation is obtained in vivo (see figure 7 below) with C5 and C2. This might be due to the cells in the microenvironment in vivo, including endometrial stromal cells, known to be important for proliferative effects on epithelia (53, 54). From these data, an EC_{50} for C2 of 14.32μM was obtained (Figure 3C). The Skp2E3LIs, C2, C20, and C5, which specifically increase nuclear p27, block pRb phosphorylation (phospho-pRb) on Ser780 by 40%, 34%, and 37%, respectively, compared with veh, in the nucleus but do not affect the levels of nuclear pRb (Figure 3D) and, accordingly, increase cells in G_1 by 13%, 11%, and 13%, respectively; C1 had little effect (Figure 3E). As shown in Figure 3F, C20, C1,C2, and C5 (10μM) were not cytotoxic after treatment of ECC-1 cells for 48 hours. However, both C16, which increases nuclear and cytoplasmic p27, and L6, which does not increase p27, induce 77% ($P \leq .001$) and 55% ($P \leq .007$) cell death, respectively. Notably, as shown in Figure 3G, whereas C2 and C20 activate caspase-3 to a similar extent as veh, in accordance with the toxicity shown for C16, this compound shows cleavage of both caspase-3 and PARP1 (markers of the final execution pathway). These data suggest that C2, C5, and C20 indeed inhibit proliferation by partitioning cells into G_1 and not by apoptosis in ECC-1 cells and, furthermore, suggest that the Skp2E3LIs, C5, C2, and C20, reduce cell proliferation by increasing nuclear p27 to block Cdk2 activity and prevent phosphorylation of pRb for cell cycle arrest. This is achieved by specifically inhibiting Skp2 E3 ligase activity without increasing cytoplasmic p27.

Skp2E3LIs, C2 and C20, block E2-induced proteasomal degradation of nuclear p27 and E2-induced proliferation

We previously showed that knocking down Skp2 in ECA cell lines completely obviated both E2-induced proliferation and degradation of nuclear (and cytoplasmic) p27 (13). This strongly suggests that the pathogenesis of E2-induced ECA is dependent on Skp2-mediated degradation of p27. As shown, both the increase in nuclear p27 (Figure 4A) and inhibition of cell proliferation (Figure 4B) by C2 and C20 are completely abrogated after knockdown of Skp2 levels (79% in cytoplasm, 82% in nucleus) in ECC-1 cells (nuclear p27: C2, 2.2-fold [$P \leq .008$]; C20, 1.8-fold [$P \leq .008$]; inhibition of proliferation: C2, 29% [$P \leq .001$]; C20, 27% [$P \leq .003$]). Furthermore, consistent with the effect of C2 and C20 in stabilizing only nuclear p27, these Skp2E3LIs only increases nuclear p27 over the veh in the control siRNA-transfected cells (Figure 4A). Taken together, these results confirm the specific inhibition of Skp2/Cks1 E3 ligase activity by these inhibitors. In addition, expectedly, knocking down Skp2 markedly increases p27 (Figure 4A and Supplemental Figure 3) and, therefore, decreases cell proliferation (by 19%) (Figure 4B). Because E2 induces p27 degradation by decreasing the E3 ligase APC/Cdh1 to spare Skp2 and Cks1 proteins from proteasomal degradation so that SCF-Skp2/Cks1 can degrade p27 (13), we show that although the classic ER blocker ICI182,780 abrogated the E2-induced 67% decrease in nuclear p27 to the level of untreated control (Figure 4C), both C2 and C20 block E2-induced degradation of p27 nearly restoring nuclear p27 levels close to the 2-fold increase over the control, as observed in Figure 1, B and C. In contrast, both C2 and C20 decrease cytoplasmic p27 levels by approximately 33%. A similar response is observed in another ECA cell line, HEC-1B (Supplemental Figure 4A). Whereas previous studies using cancer cell lines show that p27 levels are increased by Skp2E3LIs in total cell lysates (30), the fact that C2 and C20 block E2-induced degradation of nuclear p27 in ECA cells provides evidence that these Skp2E3LIs have a direct functional effect on Skp2/Cks1 E3 ligase activity, such that they inhibit proliferation. This activity underscores the potential for these inhibitors to treat complex atypical endometrial hyperplasia and prevent ECA as hyperplasia is associated with unopposed E2, which precedes type I ECA (55, 56).

Importantly, blocking E2-induced proliferation by C2 and C20 was equal to the effect of blocking ER activation with ICI182,780 (Figure 4D) in ECC-1 cells and by C2 in HEC-1B cells (Supplemental Figure 4B). The partial reversal of these Skp2E3LIs on E2-induced proliferation was statistically significant ($P \leq .022$; $P \leq .019$) and is commensurate with their ability to recover p27 levels (Figure 4C). Addition of C2 and C20 together (Figure 4E) did not further increase nuclear p27 levels, suggesting they both block the interactive pocket formed by Skp2/Cks1, for which they were originally screened by Internal Coordinate Mechanics-Virtual Ligand Screening (30). C2 and C20, as well as other Skp2E3LIs that increase p27 levels by blocking Skp2 ubiquitylating activity, have different chemical backbone scaffolds and, therefore, maximize potential for improving the compounds, including increasing probabilities for cell type-specific effects as well as for in vivo use in preclinical animal studies.

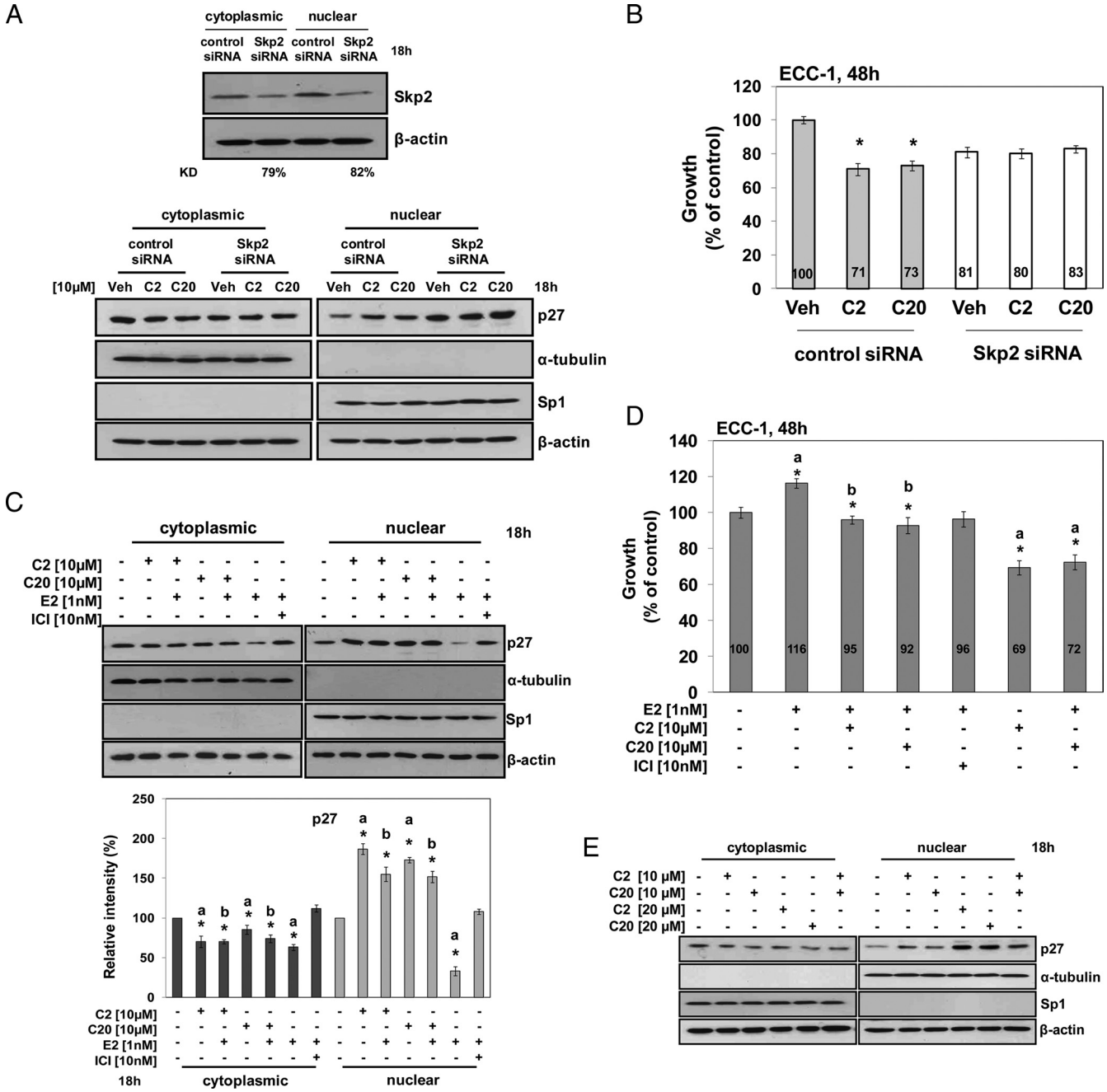

Figure 4. The Skp2E3LIs, C2 and C20, block E2-induced degradation of nuclear p27 and E2-induced proliferation in ECC-1 cells. (A) Knocking down Skp2 with *Skp2* siRNA blocks the increase in nuclear p27 induced by C2 and C20. ECC-1 cells were transfected with either control siRNA or 10nM *Skp2* siRNA, as described (13), treated with C2 and C20, and lysates analyzed (n = 2). (B) Knocking down Skp2 blocks the ability of C2 and C20 to inhibit cell proliferation. Skp2 siRNA-transfected cells were treated and analyzed for cell proliferation by MTS assay (n = 2). (C) C2 and C20 block E2-induced degradation of nuclear and cytoplasmic p27. Cells were treated as shown and analyzed by immunoblotting (n = 3). The graph shows statistical significance. a, E2, C2, and C20 compared with veh; b, C2 or C20 plus E2 compared with E2; $P \leq .001$ for all. (D) C2 and C20 block E2-induced proliferation in ECC-1 cells. Cells were treated with C2 and C20 and cell proliferation determined. Percent of control values are within the bars (n = 3). The graph shows statistical significance. a, E2 and C2, C20 compared with veh; b, C2 or C20 plus E2 compared with E2; $P \leq .001$ for all. (E) Treatment with C2 and C20 together did not further increase nuclear p27 levels than either alone (n = 3).

The Skp2E3LI, C2, stabilizes nuclear p27 while decreasing p27 in the cytoplasm in ECC-1 cells

The putative therapeutic success of Skp2E3LIs would be heightened if these compounds could increase nuclear p27 while simultaneously decreasing cytoplasmic p27; this was implicated in Figure 1C. Compared with the general proteasome inhibitor, lactacystin, which increases p27 in both the nucleus and cytoplasm (Figure 5B), C2 causes a simultaneous increase in nuclear p27 while decreasing cytoplasmic p27 over time, peaking in the nucleus at 24 hours (Figure 5A and

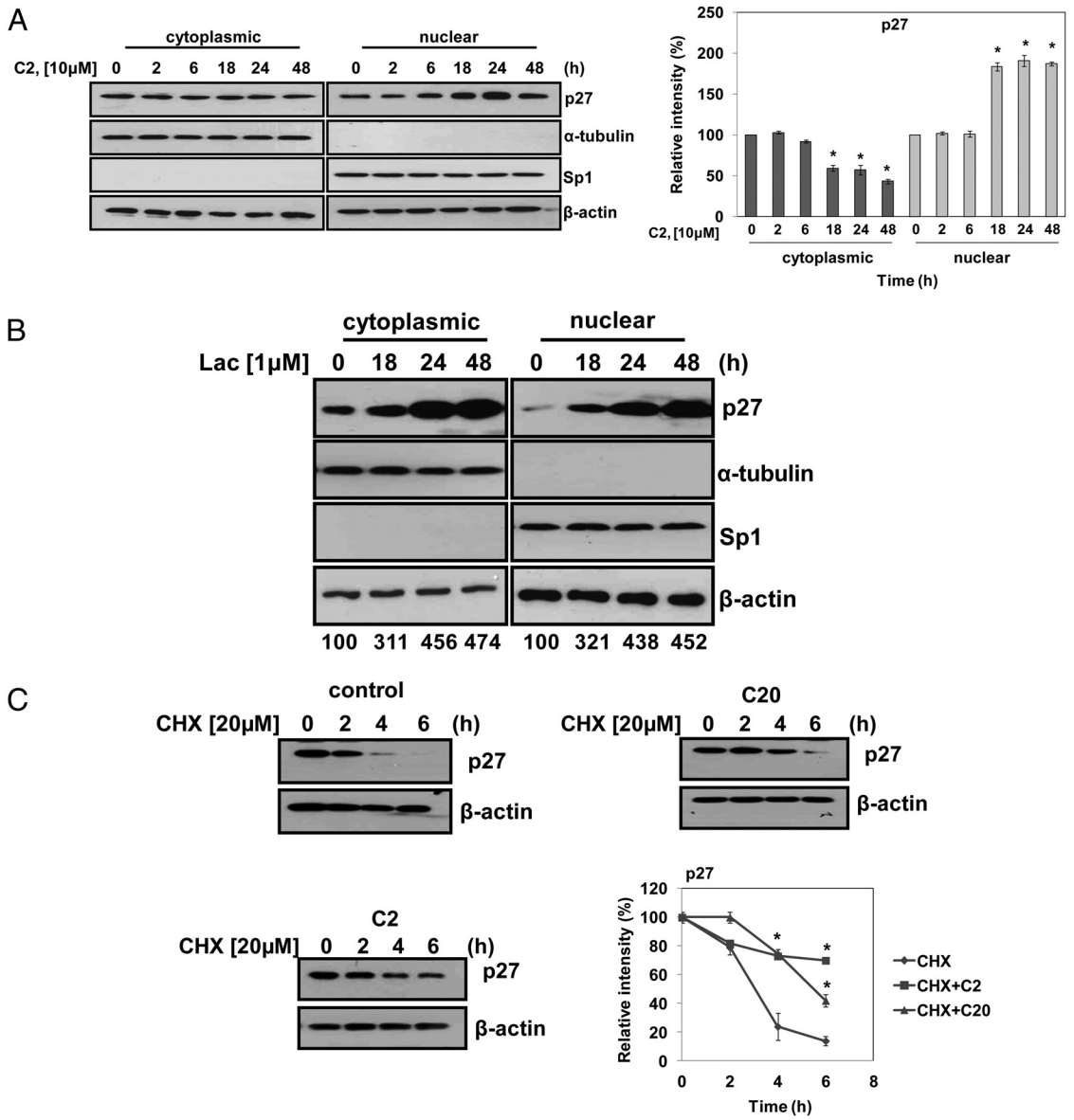

Figure 5. The Skp2E3LI, C2 increases nuclear p27 while decreasing p27 in the cytoplasm over time; C2 and C20 increase p27 half-life over controls in ECC-1 cells. (A and B) C2 stabilizes nuclear p27 and simultaneously decreases cytoplasmic p27. Lactacystin stabilizes p27 in both subcellular fractions. Cells were treated and subfractionated at the times shown. Densitometric values as percent of veh-treated are shown in the graph to the right of the blot (n = 2). (C) C2 and C20 extend p27 half-life by 6.1 and 2.7 hours over CHX control. Cells were treated with C2, C20, or veh, chased with 20μM CHX, and cell lysates collected at time points shown. The graph depicts the relative intensity of p27 levels. Statistical significance, *, $P \leq .001$ for all (n = 2).

Supplemental Figure 5). By 18 hours, the cycloheximide contained 41% ($P \leq .004$) of the level of p27, whereas nuclear p27 doubled (note, x-ray film exposure times were comparable for lactacystin and C2 at 30 s). Whereas there is a higher level of nuclear p27 in the lactacystin-treated cells, inhibition of proliferation by this reagent was similar to the Skp2E3LIs at 30%, as shown in Figure 3B. To measure the degree of p27 stabilization, we show, by incubating the cells with C2 and C20, in the presence of cycloheximide (CHX), that these inhibitors increase the half-life of p27 at 3.2 hours for control cells by 6.1 and 2.7 hours, respectively (Figure 5C). This stabilization of p27 by Skp2E3LIs is similar to previous studies, in which C20 and C16 extended the half-life of p27 to 5 and 3 hours, respectively, in the 501 melanoma cell line (30).

Skp2E3LIs stabilize nuclear p27 and decrease cytoplasmic p27 in primary ECA cells

As a step toward interrogating the potential for Skp2E3LIs as pharmacological inhibitors of p27 degradation to regain growth control in cancer, primary ECA cells were isolated from endometrioid tumors. As shown in Figure 6A, C2, C20, and C1 increase p27 levels by 1.9-, 3-, and 3.4-fold, over the veh-treated control, respectively, in primary ECA cells (grade I/III). In conjunction with an

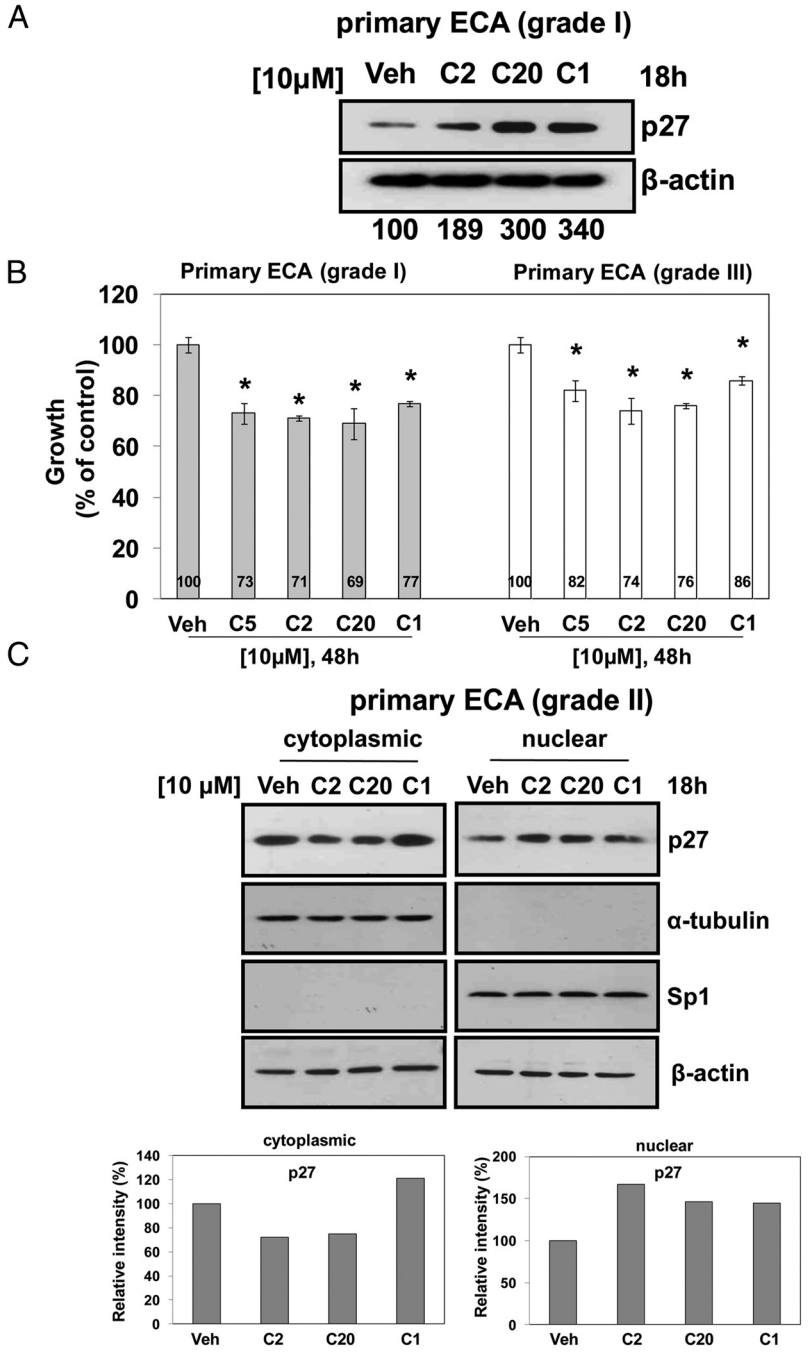

Figure 6. Skp2E3LIs inhibit cell proliferation, stabilize nuclear p27, and decrease cytoplasmic p27 in primary ECA cells isolated from fresh endometrial tissue. (A) p27 protein is increased by C2, C20, and C1 in total cell lysates of primary ECA cells derived from grade I/I endometrioid ECA. Primary ECA cells were prepared from a type I tumor, treated, and cell lysates analyzed. Densitometry values are shown at the base of the blot as percent of control. (B) Skp2E3LIs, C5, C2, C20, and C1, inhibit cell proliferation of primary ECA cells from grade III/III and I/III tumors. Proliferation was determined using the MTS assay and graphed. The values are shown within the bars on the graph; *, $P \leq .05$. (C) The Skp2E3LIs, C2 and C20, increase nuclear p27 while decreasing cytoplasmic p27 in primary ECA cells derived from a grade II/III tumor showing p27 mislocalized to the cytoplasm before treatment. Cells were treated and nuclear cytoplasmic fractions analyzed for p27. The graph represents relative intensity of p27 levels.

increase in nuclear p27, Figure 6B shows that treatment of synchronized primary ECA cells from 2 patients (I/III and III/III) with 10μM C5, C2, C20, or C1 for 48 hours caused a statistically significant inhibition of proliferation, with C2 and C20 having the strongest effect at 26% ($P \leq .0004$) and 24% ($P \leq .0001$), respectively. After subcellular fractionation of Skp2E3LI-treated primary ECA cells (grade II/III), C2 and C20 specifically decrease p27 in the cytoplasm by approximately 25% while simultaneously increasing nuclear p27 by 67% and 46%, respectively; C1 causes accumulation of p27 in both subcellular compartments (Figure 6C). The primary ECA cells shown in Figure 6C have a greater amount of cytoplasmic compared with nuclear p27 in the control, suggesting that the pathology of this patient, in part, might be cytoplasmic mislocalization of p27. Notably, C2 and C20 appear to drive accumulation of nuclear p27 from a cytoplasmic pool or possibly by increasing the degradation of p27 by the specific cytoplasmic E3 ligase, Kip1 ubiquitination promoting complex (57). An assessment of the dynamic influence of Skp2E3LIs on nuclear cytoplasmic shuttling and nuclear retention of p27 by single cell high content imaging (58–60) should provide further clues to this important putative function of C2 and other optimized Skp2E3LIs. Importantly, the proof of principle data on ECA cells from patients strongly suggests that Skp2E3LIs can be further developed as a novel therapeutic approach to block Skp2-dependent degradation of p27.

Skp2E3LIs injected into E2-primed mice stabilize nuclear p27 and decrease proliferation of EECs

As shown in Figure 7A and the graph in Figure 7B, injection of the

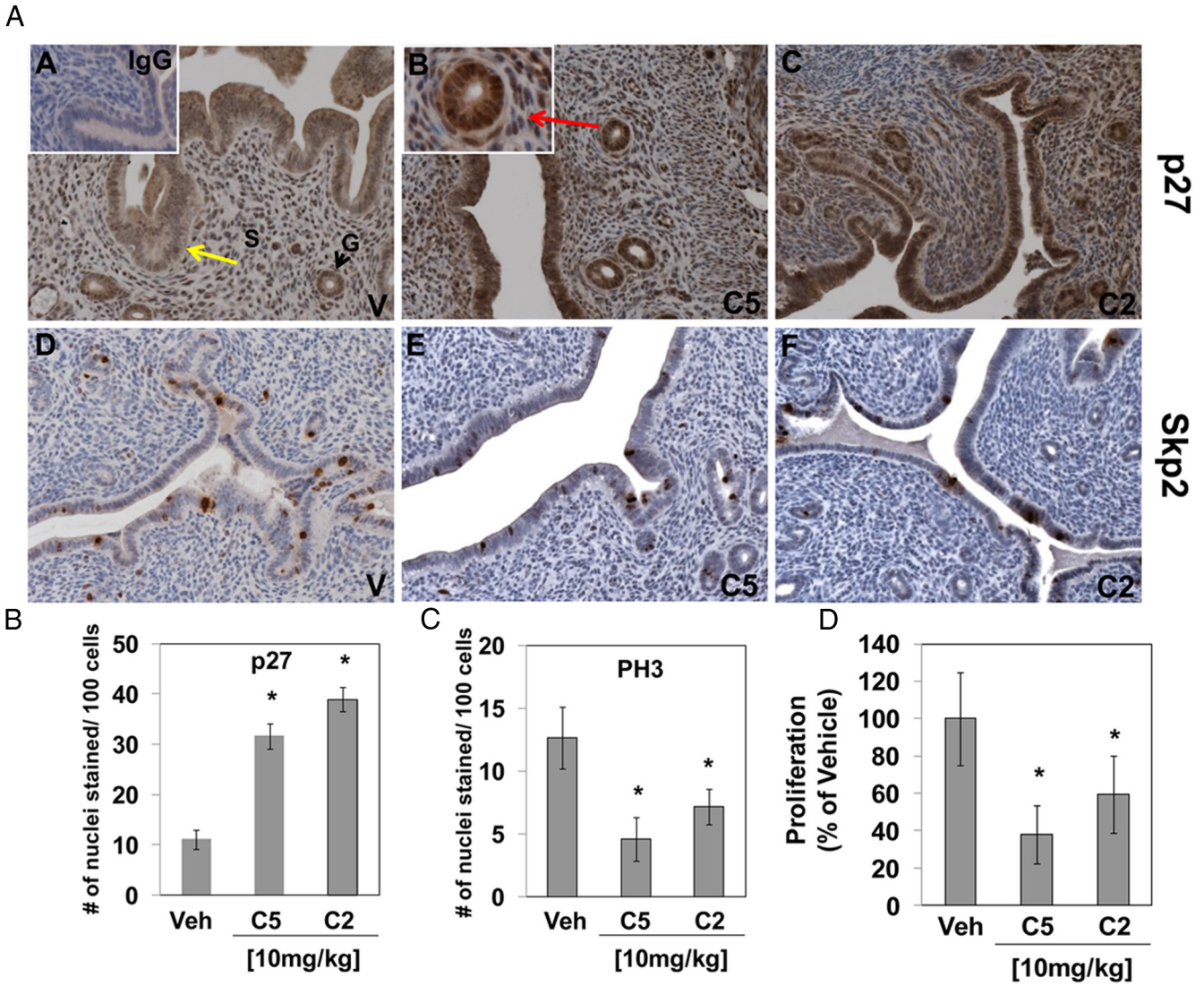

Figure 7. Skp2E3LIs, C5 and C2, injected into wild-type E2-primed mice increases nuclear p27 and decreases cell proliferation in EECs. (A) Skp2E3LIs, C5 and C2, increase p27 in the nucleus and decrease proliferation. Ovariectomized C57Bl/6 mice were treated with 100-ng E2 im for 2 days, 2 days off, injected with 10-mg/kg C5 and C2, or veh ip for 2 consecutive days and euthanized 24 hours later. IHC was performed using antibodies to mouse p27 and PH3 to detect cells undergoing mitosis. (A–C) p27 immunostained endometrium. (D–F) PH3 immunostained endometrium. Magnification is ×200 except inset panel is ×325: G, gland marked by black arrowhead (A); S, stromal cells. (B) C5 and C2 induce a statistically significant increase in nuclear p27 over veh-treated mice in EECs. The number of positively stained nuclei for p27 was counted per 100 cells in 3 separate fields. The graph illustrates the average number of nuclei stained ± SD from the tissue slides of 4 separate mice per treatment parameter. (C) C5 and C2 induce a statistically significant decrease in the number of proliferating cells over veh-treated mice by PH3 immunostaining. The data were obtained and are represented as described for graph in B. (D) C5 and C2 inhibit proliferation of mouse EECs by 42% and 62%, respectively, compared with veh-treated control mice. Values were obtained as percent of veh-treated controls set a 100. Statistical significance for B–D was estimated using the Student's *t* test.

Skp2E3LIs, C5 and C2, ip, into ovariectomized, E2-primed mice increases p27 in the nucleus of EECs (Figure 7A, panels B and C) compared with the veh-treated controls (Figure 7A) (number of nuclei/100 cells/3 fields/slide: 38.6, 31.7 compared with 11.04, respectively; C5 $P \leq .0001$ and C2 $P \leq .0001$) (Supplemental Table 1). It is notable that hyperplastic glands are present at 2 days after E2 treatment (Figure 7A, panel A, yellow arrow), whereas glandular hyperplasia was not observed in the Skp2E3LI-treated mouse EECs (Figure 7A, panels B and C), showing high nuclear p27 immunostaining (inset in Figure 7A, panel B shows intense nuclear p27 immunoreactivity in 1 cross-sectional gland; red arrow) and less intense diffuse cytoplasmic immunoreactivity; stromal cells surrounding the glands are also immunoreactive. Consistent with the higher number of cells immunostaining for nuclear p27, by PH3 positive immunostained nuclei, a statistically significant lower number of mitotic EECs is observed in the C2- and C5-treated mice (Figure 7A, panels E and F) compared with the veh-treated controls (Figure 7A, panel D)

(C5, 4.6; C2, 7.2, compared with veh, 12.6 [C5, $P \leq .002$; C2, $P \leq .008$]) (Supplemental Table 1). The data from PH3 immunostaining show that 42% and 62% inhibition of proliferation was obtained with C5 and C2, respectively ($P \leq .001$, $P \leq .002$). These studies show that the specific Skp2E3LIs, C5 and C2, can function in vivo in mice to arrest cellular proliferation ostensibly by increasing nuclear p27. Moreover, the data suggest that C5 and C2 are not acutely toxic and that and an effective dose was achieved with treatment of 10-mg/kg Skp2E3LI for 2 consecutive days. Other inhibitors of p27 degradation by Skp2 that do not affect Skp2/Cks1 E3 ligase activity have been reported (61–63). The data reported here are the first to show that the specific inhibition of SCF-Skp2/Cks1 E3 ligase activity by Skp2E3LIs increases only the tumor suppressor p27 in the nucleus and inhibits cellular proliferation in vitro and in vivo.

The studies here suggest that Skp2E3LIs might have a dual therapeutic function for ECA and other cancers first, to correct unrestrained proliferation and second, by possibly blocking metastasis when p27 is aberrantly present in the cytoplasm. Specifically, as depicted in Figure 8, we show that C2 and C20 not only increase nuclear p27, but these Skp2E3LIs also block E2-induced p27 degradation and, thereby, putatively, block E2-induced proliferation through the accumulation of nuclear p27. Simultaneously, the Skp2E3LIs, C2 and C20, are shown here to decrease cytoplasmic p27 in both ECC-1 and primary ECA cells. These inhibitors might therefore be effective in E2-induced ECA, in which p27 is both degraded in the nucleus and/or sequestered in the cytoplasm. Furthermore, their effects should be applicable to other human cancers having similar pathology of low levels of p27 and high levels of Skp2/Cks1 in the nucleus and/or high cytoplasmic p27. Because there is a need for therapies that specifically target cancer cells and are not cytotoxic for normal cells, Skp2E3LIs might selectively increase nuclear p27 to regulate growth control early in malignant progression when p27 has been shown to be lost in ECA and other cancers (1). In addition, using novel tools, such as SRFLM, to resolve subdiffraction features of molecular clusters as shown here, these inhibitors of Skp2 ubiquitylation of p27 can be used as chemical probes to map the spatial organization and interactions of nuclear cell cycle proteins during Skp2E3LI-induced G_1. Moreover, the Skp2E3LIs will allow interrogation of a single pathway linked to p27 and loss of growth control. This

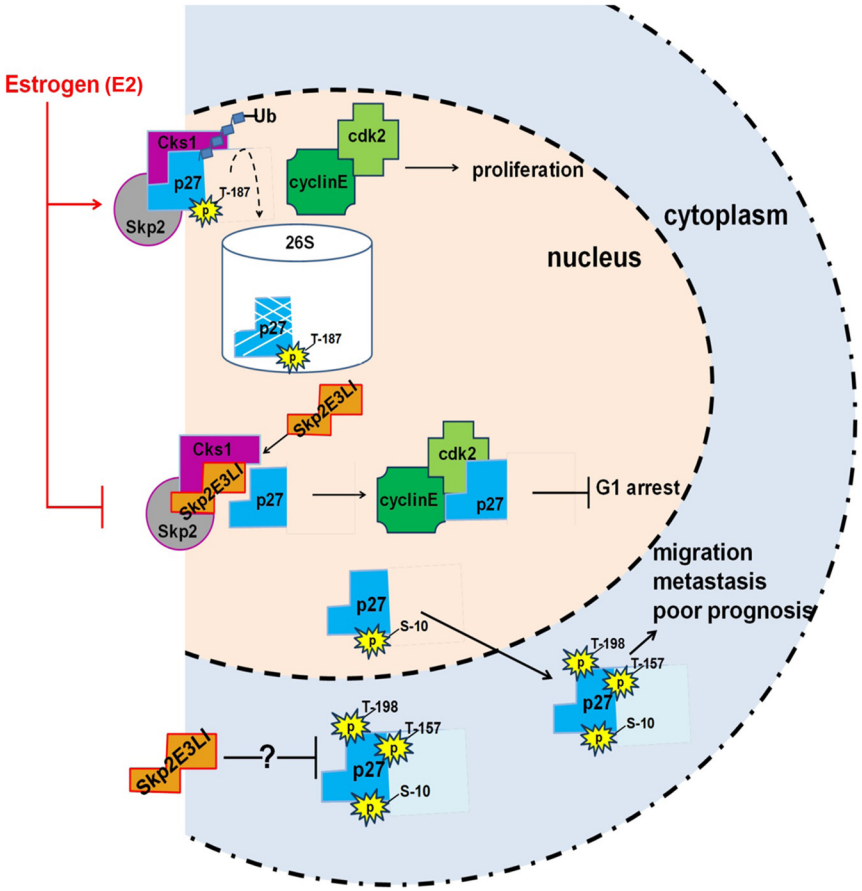

Figure 8. Skp2E3LIs stabilize nuclear p27, inhibit cell proliferation, and block E2-induced degradation of p27 and E2-induced cell proliferation in ECC-1 cells and primary ECA cells. Phosphorylation of p27 on T187 causes recognition of p27 by the SCF-Skp2/Cks1 complex and subsequent polyubiquitylation (Ub) of p27 by Skp2 in a pocket formed by the interaction of Skp2 with Cks1 (28, 29). Because ubiquitylated p27 is degraded in the 26S proteasome (26S), cyclin E/Cdk2 becomes available to enact unrestrained cell proliferation (4). Loss of nuclear p27 and increased Skp2 is characteristic of many human cancers (1, 4, 65). E2 causes p27 MAPK-mediated phosphorylation of p27 on T187 and increases Skp2 and Cks1, thereby inducing cell proliferation as a mechanism for E2-linked endometrial hyperplasia and ECA (13). The Skp2E3LIs, C5, C2, and C20, interact with the binding interface between p27 and the pocket of Skp2 interacting with Cks1 and, thus, prevent p27 from binding in the pocket (30). Then, p27 is free to bind cyclin E/Cdk2 causing G_1 arrest to harness the unrestrained proliferation of cancer cells. The Skp2E3LIs block E2-induced degradation of p27 and E2-induced proliferation and therefore are a potential novel therapeutic approach for ECA. Phosphorylation of p27 on S10 causes its export to the cytoplasm, whereas phosphorylation of p27 on T157 and T198 prevents its nuclear entry (14, 15). Cytoplasmic mislocalization of p27 allows cyclin E/Cdk2 activity for cell cycle progression and represses RhoA signaling causing cell migration and metastasis (1, 6). Skp2E3LIs increase nuclear p27 while simultaneously decreasing cytoplasmic p27 by unknown mechanisms implicating a dual positive effect as a potential therapeutic cancer agent.

was not previously possible with general proteasome inhibitors that affect the entire cell proteasomal degradation machinery, and for this same reason, these E3 ligase inhibitors represent a key advance in the use of proteasome inhibitor therapy, which have lacked the specificity to be more broadly successful as anticancer agents (64).

Acknowledgments

We thank Paraskevi Briasouli, PhD, for her help with experiments and editing.

Address all correspondence and requests for reprints to: Leslie I. Gold, PhD, Department of Medicine, Division of Translational Medicine, 550 First Avenue, NB17E4, New York, NY 10016. E-mail: leslie.gold@nyumc.org.

This work was supported by the National Institutes of Health, National Cancer Institute Grant CA 89175 and a Pilot Project grant from New York University Cancer Institute (to L.I.G.), by Office of the National Institutes of Health Director Grant OD 004631 (to T.C.), and by Advanced Medical Research Foundation and Vincent Memorial Research funds (to B.R.).

Disclosure Summary: The authors have nothing to disclose.

References

1. **Chu IM, Hengst L, Slingerland JM.** The Cdk inhibitor p27 in human cancer: prognostic potential and relevance to anticancer therapy. *Nat Rev Cancer*. 2008;8(4):253–267.
2. **Sherr CJ, Roberts JM.** CDK inhibitors: positive and negative regulators of G1-phase progression. *Genes Dev*. 1999;13(12):1501–1512.
3. **Besson A, Hwang HC, Cicero S, et al.** Discovery of an oncogenic activity in p27Kip1 that causes stem cell expansion and a multiple tumor phenotype. *Genes Dev*. 2007;21(14):1731–1746.
4. **Wander SA, Zhao D, Slingerland JM.** p27: a barometer of signaling deregulation and potential predictor of response to targeted therapies. *Clin Cancer Res*. 2011;17(1):12–18.
5. **Serres MP, Zlotek-Zlotkiewicz E, Concha C, et al.** Cytoplasmic p27 is oncogenic and cooperates with Ras both in vivo and in vitro. *Oncogene*. 2011;30(25):2846–2858.
6. **Denicourt C, Saenz CC, Datnow B, Cui XS, Dowdy SF.** Relocalized p27Kip1 tumor suppressor functions as a cytoplasmic metastatic oncogene in melanoma. *Cancer Res*. 2007;67(19):9238–9243.
7. **Larrea MD, Wander SA, Slingerland JM.** p27 as Jekyll and Hyde: regulation of cell cycle and cell motility. *Cell Cycle*. 2009;8(21):3455–3461.
8. **Chu I, Sun J, Arnaout A, et al.** p27 phosphorylation by Src regulates inhibition of cyclin E-Cdk2. *Cell*. 2007;128(2):281–294.
9. **Kelly-Spratt KS, Philipp-Staheli J, Gurley KE, Hoon-Kim K, Knoblaugh S, Kemp CJ.** Inhibition of PI-3K restores nuclear p27Kip1 expression in a mouse model of Kras-driven lung cancer. *Oncogene*. 2009;28(41):3652–3662.
10. **Chen Y, Alvarez EA, Azzam D, et al.** Combined Src and ER blockade impairs human breast cancer proliferation in vitro and in vivo. *Breast Cancer Res Treat*. 2011;128(1):69–78.
11. **Lecanda J, Parekh TV, Gama P, et al.** Transforming growth factor-β, estrogen, and progesterone converge on the regulation of p27Kip1 in the normal and malignant endometrium. *Cancer Res*. 2007;67(3):1007–1018.
12. **Bloom J, Pagano M.** Deregulated degradation of the cdk inhibitor p27 and malignant transformation. *Semin Cancer Biol*. 2003;13(1):41–47.
13. **Huang KT, Pavlides SC, Lecanda J, Blank SV, Mittal KR, Gold LI.** Estrogen and progesterone regulate p27kip1 levels via the ubiquitin-proteasome system: pathogenic and therapeutic implications for endometrial cancer. *PLoS One*. 2012;7(9):e46072.
14. **Ishida N, Hara T, Kamura T, Yoshida M, Nakayama K, Nakayama KI.** Phosphorylation of p27Kip1 on serine 10 is required for its binding to CRM1 and nuclear export. *J Biol Chem*. 2002;277(17):14355–14358.
15. **Shin I, Rotty J, Wu FY, Arteaga CL.** Phosphorylation of p27Kip1 at Thr-157 interferes with its association with importin α during G1 and prevents nuclear re-entry. *J Biol Chem*. 2005;280(7):6055–6063.
16. **Wen S, So Y, Singh K, et al.** Promotion of cytoplasmic mislocalization of p27 by Helicobacter pylori in gastric cancer. *Oncogene*. 2012;31(14):1771–1780.
17. **Liang J, Zubovitz J, Petrocelli T, et al.** PKB/Akt phosphorylates p27, impairs nuclear import of p27 and opposes p27-mediated G1 arrest. *Nat Med*. 2002;8(10):1153–1160.
18. **Kruck S, Merseburger AS, Hennenlotter J, et al.** High cytoplasmic expression of p27(Kip1) is associated with a worse cancer-specific survival in clear cell renal cell carcinoma. *BJU Int*. 109(10):1565–1570.
19. **Duncan TJ, Al-Attar A, Rolland P, Harper S, Spendlove I, Durrant LG.** Cytoplasmic p27 expression is an independent prognostic factor in ovarian cancer. *Int J Gynecol Pathol*. 2010;29(1):8–18.
20. **Hidaka T, Hama S, Shrestha P, et al.** The combination of low cytoplasmic and high nuclear expression of p27 predicts a better prognosis in high-grade astrocytoma. *Anticancer Res*. 2009;29(2):597–603.
21. **Lecanda J, Ganapathy V, D'Aquino-Ardalan C, et al.** TGFβ prevents proteasomal degradation of the cyclin-dependent kinase inhibitor p27kip1 for cell cycle arrest. *Cell Cycle*. 2009;8(5):742–756.
22. **Kane RC, Farrell AT, Sridhara R, Pazdur R.** United States food and drug administration approval summary: bortezomib for the treatment of progressive multiple myeloma after one prior therapy. *Clin Cancer Res*. 2006;12(10):2955–2960.
23. **Diefenbach CS, O'Connor OA.** Mantle cell lymphoma in relapse: the role of emerging new drugs. *Curr Opin Oncol*. 2010;22(5):419–423.
24. **Orlowski RZ, Kuhn DJ.** Proteasome inhibitors in cancer therapy: lessons from the first decade. *Clin Cancer Res*. 2008;14(6):1649–1657.
25. **Kitagawa K, Kotake Y, Kitagawa M.** Ubiquitin-mediated control of oncogene and tumor suppressor gene products. *Cancer Sci*. 2009;100(8):1374–1381.
26. **Hershko A, Ciechanover A.** The ubiquitin system. *Annu Rev Biochem*. 1998;67:425–479.
27. **Hao B, Zheng N, Schulman BA, et al.** Structural basis of the Cks1-dependent recognition of p27(Kip1) by the SCF(Skp2) ubiquitin ligase. *Mol Cell*. 2005;20(1):9–19.
28. **Cardozo T, Abagyan R.** Druggability of SCF ubiquitin ligase-protein interfaces. *Methods Enzymol*. 2005;399:634–653.
29. **Cardozo T, Pagano M.** Wrenches in the works: drug discovery targeting the SCF ubiquitin ligase and APC/C complexes. *BMC Biochem*. 2007;8(suppl 1):S9.
30. **Wu L, Grigoryan AV, Li Y, Hao B, Pagano M, Cardozo TJ.** Specific small molecule inhibitors of Skp2-mediated p27 degradation. *Chem Biol*. 2012;19(12):1515–1524.
31. **Kamata Y, Watanabe J, Nishimura Y, et al.** High expression of skp2 correlates with poor prognosis in endometrial endometrioid adenocarcinoma. *J Cancer Res Clin Oncol*. 2005;131(9):591–596.
32. **Davidovich S, Ben-Izhak O, Shapira M, Futerman B, Hershko DD.**

Over-expression of Skp2 is associated with resistance to preoperative doxorubicin-based chemotherapy in primary breast cancer. *Breast Cancer Res*. 2008;10(4):R63.
33. **Frescas D, Pagano M.** Deregulated proteolysis by the F-box proteins SKP2 and β-TrCP: tipping the scales of cancer. *Nat Rev Cancer*. 2008;8(6):438–449.
34. **Lin HK, Chen Z, Wang G, et al.** Skp2 targeting suppresses tumorigenesis by Arf-p53-independent cellular senescence. *Nature*. 2010; 464(7287):374–379.
35. **Assoian RK, Yung Y.** A reciprocal relationship between Rb and Skp2: implications for restriction point control, signal transduction to the cell cycle and cancer. *Cell Cycle*. 2008;7(1):24–27.
36. **Silverberg SG.** Hyperplasia and carcinoma of the endometrium. *Semin Diagn Pathol*. 1988;5(2):135–153.
37. **Malkusch S, Muranyi W, Müller B, Kräusslich HG, Heilemann M.** Single-molecule coordinate-based analysis of the morphology of HIV-1 assembly sites with near-molecular spatial resolution. *Histochem Cell Biol*. 2013;139(1):173–179.
38. **van de Linde S, Löschberger A, Klein T, et al.** Direct stochastic optical reconstruction microscopy with standard fluorescent probes. *Nat Protoc*. 2011;6(7):991–1009.
39. **Yamaguchi S, Reid DA, Rothenberg E, Darwin AJ.** Changes in Psp protein binding partners, localization and behaviour upon activation of the Yersinia enterocolitica phage shock protein response. *Mol Microbiol*. 2013;87(3):656–671.
40. **Hong M, Bao L, Kefaloyianni E, et al.** Heterogeneity of ATP-sensitive K+ channels in cardiac myocytes: enrichment at the intercalated disk. *J Biol Chem*. 2012;287(49):41258–41267.
41. **Chkourko HS, Guerrero-Serna G, Lin X, et al.** Remodeling of mechanical junctions and of microtubule-associated proteins accompany cardiac connexin43 lateralization. *Heart Rhythm*. 2012;9(7): 1133–1140.e1136.
42. **Tokunaga M, Imamoto N, Sakata-Sogawa K.** Highly inclined thin illumination enables clear single-molecule imaging in cells. *Nat Methods*. 2008;5(2):159–161.
43. **Lee SH, Baday M, Tjioe M, et al.** Using fixed fiduciary markers for stage drift correction. *Opt Express*. 2012;20(11):12177–12183.
44. **Baday M, Cravens A, Hastie A, et al.** Multicolor super-resolution DNA imaging for genetic analysis. *Nano Lett*. 2012;12(7):3861–3866.
45. **Rothenberg E, Ha T.** Single-molecule FRET analysis of helicase functions. *Methods Mol Biol*. 2010;587:29–43.
46. **Henriques R, Lelek M, Fornasiero EF, Valtorta F, Zimmer C, Mhlanga MM.** QuickPALM: 3D real-time photoactivation nanoscopy image processing in ImageJ. *Nat Methods*. 2010;7(5):339–340.
47. **Muggia F, Gold LI, Curtin J.** *Future Directions: New Targets*. Totowa, NJ: Humana Press, Inc; 2009.
48. **Bashir T, Pagan JK, Busino L, Pagano M.** Phosphorylation of Ser72 is dispensable for Skp2 assembly into an active SCF ubiquitin ligase and its subcellular localization. *Cell Cycle*. 2010;9(5):971–974.
49. **Boutonnet C, Tanguay PL, Julien C, Rodier G, Coulombe P, Meloche S.** Phosphorylation of Ser72 does not regulate the ubiquitin ligase activity and subcellular localization of Skp2. *Cell Cycle*. 2010; 9(5):975–979.
50. **Gao D, Inuzuka H, Tseng A, Chin RY, Toker A, Wei W.** Phosphorylation by Akt1 promotes cytoplasmic localization of Skp2 and impairs APCCdh1-mediated Skp2 destruction. *Nat Cell Biol*. 2009; 11(4):397–408.
51. **Lin HK, Wang G, Chen Z, et al.** Phosphorylation-dependent regulation of cytosolic localization and oncogenic function of Skp2 by Akt/PKB. *Nat Cell Biol*. 2009;11(4):420–432.
52. **van de Linde S, Endesfelder U, Mukherjee A, et al.** Multicolor photoswitching microscopy for subdiffraction-resolution fluorescence imaging. *Photochem Photobiol Sci*. 2009;8(4):465–469.
53. **Cunha GR, Cooke PS, Kurita T.** Role of stromal-epithelial interactions in hormonal responses. *Arch Histol Cytol*. 2004;67(5):417–434.
54. **Kurita T, Young P, Brody JR, Lydon JP, O'Malley BW, Cunha GR.** Stromal progesterone receptors mediate the inhibitory effects of progesterone on estrogen-induced uterine epithelial cell deoxyribonucleic acid synthesis. *Endocrinology*. 1998;139(11):4708–4713.
55. **Ellenson LH, Wu TC.** Focus on endometrial and cervical cancer. *Cancer Cell*. 2004;5(6):533–538.
56. **Lacey JV Jr, Chia VM.** Endometrial hyperplasia and the risk of progression to carcinoma. *Maturitas*. 2009;63(1):39–44.
57. **Kotoshiba S, Kamura T, Hara T, Ishida N, Nakayama KI.** Molecular dissection of the interaction between p27 and KPC, the ubiquitin ligase that regulates proteolysis of p27 in G1 phase. *J Biol Chem*. 2005.
58. **Szafran AT, Hartig S, Sun H, et al.** Androgen receptor mutations associated with androgen insensitivity syndrome: a high content analysis approach leading to personalized medicine. *PLoS One*. 2009;4(12):e8179.
59. **Szafran AT, Szwarc M, Marcelli M, Mancini MA.** Androgen receptor functional analyses by high throughput imaging: determination of ligand, cell cycle, and mutation-specific effects. *PLoS One*. 2008; 3(11):e3605.
60. **Ashcroft FJ, Newberg JY, Jones ED, Mikic I, Mancini MA.** High content imaging-based assay to classify estrogen receptor-α ligands based on defined mechanistic outcomes. *Gene*. 2011; 477(1–2):42–52.
61. **Rico-Bautista E, Yang CC, Lu L, Roth GP, Wolf DA.** Chemical genetics approach to restoring p27Kip1 reveals novel compounds with antiproliferative activity in prostate cancer cells. *BMC Biol*. 2010;8:153.
62. **Chan CH, Morrow JK, Li CF, et al.** Pharmacological inactivation of Skp2 SCF ubiquitin ligase restricts cancer stem cell traits and cancer progression. *Cell*. 2013;154(3):556–568.
63. **Ungermannova D, Lee J, Zhang G, Dallmann HG, McHenry CS, Liu X.** High-throughput screening AlphaScreen assay for identification of small-molecule inhibitors of ubiquitin E3 ligase SCFSkp2-Cks1. *J Biomol Screen*. 2013;18(8):910–920.
64. **Rico-Bautista E, Wolf DA.** Skipping cancer: small molecule inhibitors of SKP2-mediated p27 degradation. *Chem Biol*. 2012;19(12): 1497–1498.
65. **Gstaiger M, Jordan R, Lim M, et al.** Skp2 is oncogenic and overexpressed in human cancers. *Proc Natl Acad Sci USA*. 2001;98(9): 5043–5048.